



Early Jurassic paleoclimate in Southwest China and its implications for dinosaur fossil distribution

Huan Shen, Laiming Zhang, Chengshan Wang, Romain Amiot, Xu Wang, Linlin Cui, Peng Song

► To cite this version:

Huan Shen, Laiming Zhang, Chengshan Wang, Romain Amiot, Xu Wang, et al.. Early Jurassic paleoclimate in Southwest China and its implications for dinosaur fossil distribution. Geological Journal, In press, <10.1002/gj.4168>. <hal-03374063>

HAL Id: hal-03374063

<https://hal.science/hal-03374063v1>

Submitted on 11 Oct 2021

HAL is a multi-disciplinary open access archive for the deposit and dissemination of scientific research documents, whether they are published or not. The documents may come from teaching and research institutions in France or abroad, or from public or private research centers.

L'archive ouverte pluridisciplinaire **HAL**, est destinée au dépôt et à la diffusion de documents scientifiques de niveau recherche, publiés ou non, émanant des établissements d'enseignement et de recherche français ou étrangers, des laboratoires publics ou privés.



HAL Authorization

Geological Journal

Early Jurassic paleoclimate in Southwest China and its implications for dinosaur fossil distribution

Journal:	<i>Geological Journal</i>
Manuscript ID	GJ-20-0472
Wiley - Manuscript type:	Research Article
Date Submitted by the Author:	28-Nov-2020
Complete List of Authors:	Shen, Huan; China University of Geosciences Beijing, School of Earth Science and Resources Zhang, Laiming; China University of Geosciences Beijing, Wang, Chengshan; China University of Geosciences Beijing, School of the Earth Science and Resources Amiot, Romain ; Université Claude Bernard Lyon 1, Planètes et Environnement Wang, Xu; Chinese Academy of Sciences, Institute of Geology and Geophysics Cui, Lin; Chinese Academy of Sciences, Institute of Geology and Geophysics Song, Peng; National Institute of Natural Hazards
Keywords:	Early Jurassic, dinosaur fossils, Lufeng, stable isotope geochemistry, apatite

SCHOLARONE™
Manuscripts

1 **Early Jurassic paleoclimate in Southwest China and its**
2 **implications for dinosaur fossil distribution**

3
4 Huan Shen ¹, Laiming Zhang ^{1*}, Chengshan Wang ^{1*}, Romain Amiot ², Xu Wang ³,
5 Linlin Cui ³, Peng Song ⁴

6 ¹ State Key Laboratory of Biogeology and Environmental Geology, China University of
7 Geosciences, Beijing 100083, China, and School of the Earth Science and Resources, China
8 University of Geosciences, Beijing 100083, China

9 ² Univ Lyon, Univ Lyon 1, ENSL, CNRS, LGL-TPE, F-69622 Villeurbanne, France

10 ³ Key Laboratory of Cenozoic Geology and Environment, Institute of Geology and Geophysics,
11 Chinese Academy of Sciences, Beijing 100029, China

12 ⁴ National Institute of Natural Hazards, MEMC, Beijing 100085, China

13
14 Corresponding author: lzhang@cugb.edu.cn and chshwang@cugb.edu.cn

15
16 **Abstract**

17 Lufeng County in Southwest China is one of the most famous lagerstätten in which
18 Early Jurassic dinosaurs can be found. The reason of burial for large body size
19 dinosaur fossils at this site is still an enigma, although it could be attributed to either
20 suitable habitats or good preservation conditions. Both of these factors are indirectly
21 regulated by climatic conditions. Therefore, a quantitative reconstruction of the
22 terrestrial paleoclimate of the Lufeng area during the Early Jurassic could help shed
23 new light on this issue. In this study, we analysed the stable isotope compositions of
24 oxygen and carbon ($\delta^{13}\text{C}$ and $\delta^{18}\text{O}$) in apatite phosphate and carbonate from the tooth

enamel and compact bones of basal sauropodiform and *Sinosaurus* fossils. The oxygen isotopes provided a mean air temperature (MAT) of $\geq 21 \pm 3^{\circ}\text{C}$, and the carbon isotopes allowed us to estimate a mean annual precipitation (MAP) of 965 ± 460 mm/yr during the Early Jurassic in Lufeng County. These conditions correspond to a relatively arid tropical savanna climate hospitable to vertebrates life. We also compared the spatial relationship between the global distribution of dinosaur fossils and climatically sensitive deposits during the Jurassic. The dinosaur fossil distribution reveals a strong preference for arid regions. We therefore suggest that “savanna-like” tropical conditions helped accommodate a large number of dinosaurs and preserve their carcasses in the Lufeng area during the Early Jurassic.

Keywords: Early Jurassic; dinosaur fossils; Lufeng; stable isotope geochemistry; apatite

1 Introduction

Lufeng County, Yunnan Province, located in southwestern China, holds the main sites of Early Jurassic vertebrate fossils (Fang et al., 2000; Galton & Upchurch, 2004). In this region, several localities have yielded a rich and diverse dinosaur fauna, including non-sauropodan basal sauropodomorphs (Sun & Cui, 1986; Wang, You & Wang, 2017). At least 200 basal sauropodomorph dinosaur individuals belonging to five genera have been excavated, which makes Lufeng County one of the most famous lagerstätten containing Early Jurassic dinosaur fossils in the world (Barrett, Upchurch, & Wang, 2005, 2007a; Langer, Bittencourt, & Schultz, 2010; Wang et al.,

1
2
3
4
5
6
7
8
9
10
11
12
13
14
15
16
17
18
19
20
21
22
23
24
25
26
27
28
29
30
31
32
33
34
35
36
37
38
39
40
41
42
43
44
45
46
47
48
49
50
51
52
53
54
55
56
57
58
59
60

2017; Young, 1941a, 1941b, 1942, 1947, 1951 ; Zhang & Yang, 1995). In addition, other vertebrate fossils such as turtles, lizards, crocodylomorphs, therapsids and mammals, have also been found, indicating the high biodiversity and environmental suitability in this region during the Early Jurassic (Chow & Hou, 1959; Chow, 1962; Crompton & Sun, 1985; Dong, 1990; Hopson, 1964; Patterson & Olson, 1961; Rigney, 1963; Simmons, 1965; Sun & Cui, 1986; Wu, 1991; Wu & Chatterjee, 1993; Zhang & Cui, 1983). The fossils in Lufeng County are also famous for their completeness and exceptional preservation conditions (Luo & Wu, 1994; Young, 1941a). The reason for this large-scale burial of well-preserved dinosaur fossils is of great interest; however, few studies on the subject have been conducted to address this issue. Both the living and burial environments for these vertebrates would be highly regulated or affected by the local paleoclimate. By using an ecological structure analysis, previous studies have claimed that more arid environments tend to favour the preservation of a greater proportion of large-bodied taxa and tend to lack taxa weighing less than 10 kg during the Late Jurassic (Noto & Grossman, 2010). Therefore, it is essential to reconstruct the paleoclimate in Lufeng County during the Early Jurassic to assess this possible taphonomic bias.

The stable oxygen and carbon isotope compositions of mineralized remains of vertebrates (i.e., teeth and bones) can be used to infer their ecological and living environmental conditions (Amiot et al., 2015, 2017; Cullen et al., 2020). The oxygen isotope composition of apatite phosphate ($\delta^{18}\text{O}_\text{p}$) from terrestrial vertebrate bones and teeth is a function of the oxygen isotope composition of the animal's body water

($\delta^{18}\text{O}_{\text{bw}}$) as well as that of its body temperature (Amiot et al., 2006; Fricke & Rogers, 2000; Kolodny, Luz, & Navon, 1983; Longinelli, 1984; Luz, Kolodny, & Horowitz, 1984). For most vertebrates, the $\delta^{18}\text{O}_{\text{bw}}$ value is related to the $\delta^{18}\text{O}$ value of ingested water, mainly from plants and drinking water, which is ultimately derived from meteoric water and modified by the animals' physiology and ecology (Kohn, Schoeninger, & Valley, 1996; Straight, Barrick, & Eberth, 2004). The $\delta^{18}\text{O}$ value of meteoric water is influenced by temperature, humidity, and the amount of precipitation (Dansgaard, 1964; Fricke & O'Neil, 1999; Grafenstein, Erlenkeuser, Mueller, Trimborn, & Alefs, 1996). Therefore, the climate conditions under which the dinosaurs lived could be recorded in the stable oxygen isotope composition of the apatite phosphate in their skeletal records.

The carbon isotope composition of apatite carbonate ($\delta^{13}\text{C}_{\text{c}}$) from terrestrial vertebrate teeth or bones is related to the carbon isotope composition of ingested food, with heavy isotope enrichment that varies depending on the digestive physiology of the animal (Passey et al., 2005). For plant-eating vertebrates, the $\delta^{13}\text{C}$ value of the apatite carbonate in their teeth and bones reflects that of their plant diet ($\delta^{13}\text{C}_{\text{leaf}}$). It is thus possible to estimate the $\delta^{13}\text{C}_{\text{leaf}}$ value from the $\delta^{13}\text{C}_{\text{c}}$ values of plant-eating vertebrate teeth or bones. Combined with the established relationship between the $\delta^{13}\text{C}_{\text{leaf}}$ value of extant C_3 plants and mean annual precipitation (MAP), MAP values can be inferred from the apatite carbonate $\delta^{13}\text{C}_{\text{c}}$ values of vertebrates (Amiot et al., 2015). In this study, we apply these oxygen and carbon isotope proxies to dinosaur teeth and bones from Lufeng County to reconstruct the Early Jurassic paleoclimatic

1
2
3
4
5
6
7
8
9
10
11
12
13
14
15
16
17
18
19
20
21
22
23
24
25
26
27
28
29
30
31
32
33
34
35
36
37
38
39
40
41
42
43
44
45
46
47
48
49
50
51
52
53
54
55
56
57
58
59
60

91 conditions in terms of mean air temperature and mean amount of precipitation.

92 In this study, we also examine the spatial relationships between the global

93 distribution of dinosaur fossils and climatically sensitive deposits to explore the

94 climatic (arid and humid) preference of Jurassic dinosaurs. Proxies based on

95 climatically sensitive deposits have been widely applied to estimate arid and humid

96 regimes (Boucot, Xu, & Scotese, 2013; Porada et al., 2016; Torsvik & Cocks, 2016;

97 William & Sascha, 2012; Zhang et al., 2016). For example, the formation of coal

98 needs abundant rainfall and usually develops under specific climatic conditions, such

99 as in tropical rainforests or temperate forests (Craggs, Valdes, & Widdowson, 2012;

100 Izart et al., 2012; Utescher, Ashraf, Kern, & Mosbrugger, 2020). We believe that the

101 combination of a local quantitative terrestrial paleoclimate reconstruction and the

102 analysis of the global qualitative spatial contrast between the global distribution of

103 dinosaur fossils and climatically sensitive deposits using ArcGIS software during the

104 Jurassic could help to shed new light on the enigma of the burial of large quantity of

105 dinosaur fossils.

107 **2 Geological setting**

108 Lufeng Basin, Yunnan Province, Southwest China (25.15 °N, 102.08 °E) was

109 located between 30° N and 40° N during the Early Jurassic (Huang, 2005) (Figure 1).

110 It is a back-arc basin caused by the subduction-collision of the Yangtze Block during

111 the Late Triassic-Jurassic (Chen, Hu, Qu, & Wu, 2011). The sedimentary sequence

112 preserved in the Lufeng Basin comprises the Lower Jurassic Lufeng Formation (the

Shawan and Zhangjia'ao members), the Middle Jurassic Chuanjie and Laoluocun members, and the Upper Jurassic Madishan and Anning members, from bottom to top (Fang et al. 2000; Huang, 2005; Figure 2). The fine-grained sediments of the Lufeng Formation contain a large number of Early Jurassic dinosaur fossils. It is characterized by red and purple-red fine-grained sediments with small amounts of interlayer limestone (Figure 2), which represents a shallow lacustrine environment. The widespread paleosol carbonate nodules suggest an arid or semiarid climate during the deposition of the Lufeng Formation. Starting at the beginning of the 1940s, numerous dinosaur fossils, as well as footprints, have been collected in Lufeng Basin. These dinosaur fossils are relatively well preserved and densely distributed, and the Lufeng Formation includes for the sauropodomorphs *Lufengosaurus* (Barrett et al., 2005; Young 1941a, 1951), *Yunnanosaurus* (Barrett et al. 2007b; Young 1942), *Jingshanosaurus* (Zhang & Yang, 1995), and *Xixiposaurus* (Sekiya, 2010), an unnamed basal sauropod (= "Yizhousaurus"; Chatterjee et al., 2010), and some theropods (e.g., Hu, 1993; Wu, Currie, Dong, Pan, & Wang, 2009) and ornithischians (e.g., Irmis & Knoll 2008).

129

130 3 Material and methods

131 3.1 Material

132 In this study, two teeth and two bones collected from the Lufeng Formation were
133 analysed¹ (Table 1). The studied samples consist of two bones (LFB01 and LFB02)

¹ The fossils were donated by the Lufeng Dinosaurian Museum.

1
2
3
4
5
6
7
8
9
10
11
12
13
14
15
16
17
18
19
20
21
22
23
24
25
26
27
28
29
30
31
32
33
34
35
36
37
38
39
40
41
42
43
44
45
46
47
48
49
50
51
52
53
54
55
56
57
58
59
60

134 and one tooth (LFT06) of a basal sauropodiform and one tooth (ZGT09) of the
135 theropod *Sinosaurus triassicus*. The tooth of the herbivorous basal sauropodiform
136 shows a typical “flat and blunt leaves” shape since its primary function was grinding,
137 cutting, or shearing (Galton, 1985; Figure 3). The tooth of the carnivore *Sinosaurus*
138 (Dinosauria: Theropoda) has typical predatory/scavenger characteristics with fine
139 serrations at the edges (Xing et al., 2013).

140 The well-preserved hard parts of the teeth and compact bones were powdered by
141 using a dental drill. For each bone, powders drilled from different locations were
142 mixed. For each tooth, the powder from the apex and cervix were collected and
143 analysed separately.

144

145 **3.2 Methods**

146 **3.2.1 Measurements of oxygen and carbon isotope compositions of apatite**
147 **phosphate and carbonate**

148

149 Apatite powders from dinosaur teeth and bones were treated following the
150 protocol described in Lécuyer (2004). This protocol consists of the isolation of
151 phosphate (PO_4^{3-}) from apatite as silver phosphate (Ag_3PO_4) crystals using acid
152 dissolution and an anion-exchange resin. For each sample, 20-30 mg of enamel
153 powder was dissolved in 2 mL of 2 M HF. The CaF_2 residue was separated by
154 centrifugation and the solution was neutralized by adding 2.2 mL of 2 M KOH.
155 Amberlite™ anion-exchange resin beads were added to the solution to isolate the

1
2
3
4 156 PO_4^{3-} ions. After 24 h, the solution was removed, and the resin was rinsed and eluted
5
6
7 157 with 27.5 mL of 0.5 M NH_4NO_3 . After 4 h, 0.5 mL of NH_4OH and 15 mL of an
8
9 158 ammonia solution of AgNO_3 were added, and the solutions were placed in a
10
11
12 159 thermostatic bath at 70°C for 7 h, allowing the precipitation of Ag_3PO_4 crystals. The
13
14
15 160 oxygen isotope compositions of the silver phosphate crystals were measured using a
16
17 161 high temperature elemental analyser equipped with “purge and trap” technology
18
19
20 162 interfaced in continuous flow mode to an isotopic ratio mass spectrometer at the
21
22 163 Laboratoire de Géologie de Lyon (UMR 5276, Université Claude Bernard Lyon 1).
23
24
25 164 For each sample, 5 aliquots of 300 μg of Ag_3PO_4 were mixed with 300 μg of pure
26
27 165 graphite powder loaded in silver foil capsules. Pyrolysis was performed at 1450°C
28
29
30 166 with a glassy carbon reactor using a varioPYROcube™ Elemental Analyser interfaced
31
32
33 167 in continuous flow mode with an Isoprime™ isotopic ratio mass spectrometer. The
34
35 168 measurements were calibrated against silver phosphate precipitated from NBS120c
36
37
38 169 (natural Miocene phosphorite from Florida), as well as against NBS127 (barium
39
40 170 sulfate precipitated using seawater from Monterey Bay, California, USA). The value
41
42
43 171 of NBS120c was fixed at 21.7‰ (V-SMOW; Vienna Standard Mean Ocean Water)
44
45 172 according to [Lécuyer, Grandjean, O'Neil, Capetta, and Martineau. \(1993\)](#), and that of
46
47
48 173 NBS127 set at the value of 9.3‰ V-SMOW ([Hut, 1987](#)) for the correction of the
49
50
51 174 instrumental mass fractionation during CO isotopic analysis. The silver phosphate
52
53 175 precipitated from the standard NBS120c along with the silver phosphate samples
54
55
56 176 derived from the fossil bioapatites was repeatedly analysed ($\delta^{18}\text{O}_\text{p} = 21.7 \pm 0.1\text{‰}$, n =
57
58
59 177 4) to ensure that no isotopic fractionation occurred during the wet chemistry. Data are
60

178 reported as $\delta^{18}\text{O}$ values vs. V-SMOW (in ‰ δ units).

179 Approximately 10 mg of enamel, or bone powder was pre-treated according to
180 the procedure of Koch, Tuross, and Fogel. (1997). To remove organic matter and
181 dibasic carbonates, the powder was cleaned with a 2% NaOCl solution followed by
182 being treated using a 0.1 M acetic acid solution. Each treatment lasted for 24 h. The
183 samples were rinsed five times with distilled water. Afterward, at Laboratory for
184 Environment Isotope Geochemistry, Institute of Geology and Geophysics, Chinese
185 Academy of Sciences, the samples were analysed using a Thermo Finnigan Gasbench
186 II coupled with MAT253 continuous flow isotope ratio mass spectrometer, following
187 a procedure adapted from the methods outlined in Spoetl and Vennemann (2003).
188 Five drops of 100% orthophosphoric acid were added and the samples were allowed
189 to react at 72°C in helium for 1 h. After that, 10 measurements of the isotopic
190 composition of the resulting carbon dioxide. The measured carbon and oxygen
191 isotopic compositions were normalized relative to the NBS-19 calcite standard with
192 the addition of calcite CO_2 -carbonate acidic fractionation factors. The reproducibility
193 of the carbon and oxygen isotope compositions of the carbonate apatite was better
194 than $\pm 0.1\text{‰}$ and $\pm 0.2\text{‰}$, respectively. The carbon and oxygen isotopic compositions
195 are reported relative to the V-PDB and V-SMOW, respectively (in ‰ δ units).

196

197 3.2.2 Data compilation of dinosaur fossils and climatically sensitive deposits

198 Using the Paleobiology Database (<https://paleobiodb.org/>), a dataset of Jurassic
199 dinosaur fossil sites was compiled (Appendix 1). This study focuses on the burial

environments of fossil bones, excluding dinosaur eggs and tracks in this data compilation. These fossil sites are classified into two groups according to their stratigraphic age (i.e., Lower-Middle Jurassic and Upper Jurassic). The paleolatitude and paleolongitude for each site provided by the database were also used.

Climatically sensitive deposit markers corresponding to two time slices, the Early-Middle Jurassic and the Late Jurassic were compiled from the Lithologic Atlas according to [Boucot et al. \(2013\)](#). In our compilation, evaporites, gypsums, and calcretes were regarded as arid indicators, while coals seam were regarded as humid indicators. The paleolatitude and paleolongitude during the Early-Middle Jurassic (180 Ma) and Late Jurassic (150 Ma) for each deposit are calculated by using PointTracker software.

Each locality was plotted on a paleogeographic map (180 and 150 Ma reconstructions) using PALEOMAP PaleoAtlas raster mapping in ArcGIS software.

4 Results

4.1 Oxygen and carbon isotope compositions of apatite phosphate and carbonate

For the basal sauropodiforms, the $\delta^{18}\text{O}_p$ values ranged from 15.9‰ to 20.5‰ with an average value of 17.6 ± 0.2 ‰, and the $\delta^{13}\text{C}_c$ values ranged from -10.6‰ to -8.7‰, with an average value of -9.5 ± 0.1 ‰. For the *Sinosaurus* specimens, the $\delta^{18}\text{O}_p$ values ranged from 17.0‰ to 20.4‰, with an average value of 18.7 ± 0.2 ‰, and the $\delta^{13}\text{C}_c$ values ranged from -7.8‰ to -7.1‰, with an average value of -7.4 ± 0.1 ‰ (Table 1).

1
2
3
4
5
6
7
8
9
10
11
12
13
14
15
16
17
18
19
20
21
22
23
24
25
26
27
28
29
30
31
32
33
34
35
36
37
38
39
40
41
42
43
44
45
46
47
48
49
50
51
52
53
54
55
56
57
58
59
60

222

223 **4.2 The distribution of dinosaur fossils and climatically sensitive deposits**

224 In our database, 594 fossil sites and 829 climatically sensitive deposit markers
225 were compiled (Appendix 1; Figure 4).

226 For the Early-Middle Jurassic, 408 dinosaur fossil sites and 591 climatically
227 sensitive deposit markers were compiled. The arid zones occurred in southern North
228 America, most of South America, and the majority of Africa and the Persian Gulf
229 region. There were also scattered arid areas in South Asia. Humid belts are prominent
230 at higher latitudes of the Northern Hemisphere and in Australia in the Southern
231 Hemisphere. The dinosaur fossils are mostly distributed at middle and low latitudes,
232 including in southern North America and in the shallow continental shelves of South
233 America and Africa, with scattered fossil sites in central Asia. However, at mid- and
234 high latitudes, dinosaur fossils are scarce. We noticed that the majority of dinosaur
235 fossil sites were associated with arid climatic markers, especially in southern North
236 America and northern South America.

237 For the Late Jurassic, 186 dinosaur fossil sites and 238 climatically sensitive
238 deposit sites were collected. A Northern Hemisphere arid belt that extends from
239 eastern North America through southern Russia, Central Asia, and parts of
240 southwestern and northern China to southern England can be observed. This arid belt
241 is also a major zone for dinosaur fossil occurrences. The humid zone is mainly located
242 in South America, Australia, the Indian Peninsula, and southern South America, in a
243 state of dissimilarity with most dinosaur fossil sites. The dinosaur fossils are mainly

distributed in middle and lower latitudes, especially at the regions near the equator (Figure 4).

5 Discussion

5.1 Preservation of dinosaur teeth and bone stable isotope compositions

The stable oxygen and carbon isotope compositions of vertebrate remains can be altered by the diagenetic conditions (e.g., fracturing, fluid circulation, and metamorphism) and chemical properties (e.g., temperature, pH, and Eh) of the burial environment. Diagenetic alteration mainly occurs through the dissolution-precipitation mechanism, which can be either microbially mediated or induced by mineral-fluid interactions (Lécuyer, Grandjean, & Sheppard, 1999; Zazzo, Lécuyer, & Mariotti, 2004a). Compared to other vertebrate remains, enamel is more reliable and prone to resisting diagenetic alteration as a result of its larger and more densely packed apatite crystals, lower organic matter content, and lower porosity (Fricke & Pearson, 2008; Stanton-Thomas & Carlson, 2004). In addition, it has been shown that compact bone can also be a reliable material used to archive original isotopic compositions (Kohn & Cerling, 2002; Longinelli, 1984; Luz et al., 1984; Tütken, Pfretzschner, Vennemann, Sun, & Wang, 2004).

In the case of equilibration with diagenetic fluids, it would be expected that the isotopic compositions of different taxa would tend to homogenize towards the value of the diagenetic source. Lécuyer et al. (2003) suggested that the original information could be altered if the difference between the isotopic values of different taxa is less

1
2
3
4
5
6
7
8
9
10
11
12
13
14
15
16
17
18
19
20
21
22
23
24
25
26
27
28
29
30
31
32
33
34
35
36
37
38
39
40
41
42
43
44
45
46
47
48
49
50
51
52
53
54
55
56
57
58
59
60

than 1‰. In this study, the difference between isotopic values of the basal sauropodiform and *Sinosaurus* is larger than 1‰, which suggests that our samples were not homogenized during burial.

Based on a summary of the isotopic values of the teeth and bones of modern vertebrates, [Rey, Amiot, and Fourel \(2017\)](#) proposed a method to distinguish vertebrate remains that have preserved their stable oxygen isotope composition of apatite. First, inorganic carbonate precipitated from diagenetic fluids would lead to a carbonate content in apatite higher than 13.4%, as the naturally occurring apatite-bound carbonate content of extant vertebrates does not exceed this value ([Rey et al., 2017](#)). Second, microbially-mediated diagenetic alteration of apatite phosphate leads to a difference between $\delta^{18}\text{O}_p$ and $\delta^{18}\text{O}_c$ exceeding 14.7‰ ([Vennemann, Hegner, Cliff, & Benz, 2001](#); [Zazzo, Lécuyer, Sheppard, Grandjean, & Mariotti, 2004b](#); Figure 5). In this study, all the $\delta^{18}\text{O}_p - \delta^{18}\text{O}_c$ values were lower than 14.7‰ and the carbonate contents of our samples were less than 13.4% (Figure 3). Therefore, we suggest that our samples have at least partially maintained their original oxygen and carbon isotope compositions and could be interpreted in terms of the paleoecology and living environment of the Early Jurassic dinosaurs in Lufeng County.

5.2 Early Jurassic terrestrial paleoclimate in Lufeng County

5.2.1 Temperature and precipitation

The $\delta^{18}\text{O}$ value of meteoric water ($\delta^{18}\text{O}_w$), which constitutes a major source of drinking water for terrestrial vertebrates can be used to calculate the mean air

temperature using a modern relationship relating the mean $\delta^{18}\text{O}_w$ value of precipitation to the mean annual air temperature (MAAT), such as the relationship proposed in [Amiot et al. \(2004\)](#):

$$\delta^{18}\text{O}_w = 0.49(\pm 0.03) \times T - 14.18(\pm 0.52) \quad (1)$$

with T being the MAAT value in °C. Using the phosphate-water oxygen isotope fractionation equation established for extant vertebrates, it is possible to estimate the $\delta^{18}\text{O}_w$ value of meteoric water from the $\delta^{18}\text{O}_p$ value of apatite phosphate. For dinosaurs, the $\delta^{18}\text{O}$ value of meteoric water ($\delta^{18}\text{O}_w$) could be estimated using the present-day relationships established between birds, the closest living relatives to dinosaurs, and meteoric water (equation 2; [Amiot et al., 2017](#)); this estimation has been recently tested on Cretaceous dinosaurs ([Amiot et al., 2020](#)).

$$\delta^{18}\text{O}_w = 1.119(\pm 0.04) \times \delta^{18}\text{O}_p - 24.222(\pm 0.644) \quad R^2 = 0.98 \quad (2)$$

In this study, the average $\delta^{18}\text{O}_p$ value is $18.2 \pm 0.1\text{‰}$. Using equation 1, the average $\delta^{18}\text{O}_w$ value is $-3.9 \pm 0.94\text{‰}$. Assuming that the meteoric water cycle of the Early Jurassic did not differ drastically compared with the modern cycle, the modern relationship between the mean annual air temperature (MAAT) and $\delta^{18}\text{O}_w$ value (equation 2) can be applied to provide a temperature value for the Early Jurassic in Lufeng County of $21 \pm 3^\circ\text{C}$ (Table 2).

According to [Diefendorf, Mueller, Wing, Koch, and Freeman. \(2010\)](#), a significant relationship exists between the average $\delta^{13}\text{C}$ values of C_3 plants and the local mean annual precipitation (equation 3):

$$\log_{10}(\text{MAP}) = 0.0802(\pm 0.0102) \times \delta^{13}\text{C}_{\text{leaf}} + 1.3726(\pm 0.1875); \quad R^2 = 0.44 \quad (3)$$

with $\Delta^{13}\text{C}_{\text{leaf}} = (\delta^{13}\text{C}_{\text{atm}} - \delta^{13}\text{C}_{\text{leaf}}) / (1 + \delta^{13}\text{C}_{\text{leaf}}/10^3)$. To estimate an average $\delta^{13}\text{C}$ value for local plants, the $\delta^{13}\text{C}_c$ value of apatite carbonate from the teeth and bones of herbivorous dinosaurs can be used by applying the carbonate-diet ^{13}C enrichment established for plant-eating animals. Using the carbon isotope compositions of the plant-derived organic matter of the sediment bearing dinosaur teeth, [Tütken \(2011\)](#) estimated an apatite-diet ^{13}C -enrichment close to 16‰ for sauropods. Although their phylogenetic position is still debated, basal sauropodiforms are believed to be the ancestors of sauropods ([Barrett et al., 2005](#)). Therefore, we assume in this study that the carbon isotope fractionation between local plants and basal sauropodiform apatite is 16‰. In this way, the inferred $\delta^{13}\text{C}$ values of the diet (plants) of basal sauropodiform range from -28.8‰ to -23.8‰, which is consistent with the $\delta^{13}\text{C}$ values of modern C_3 plants (-20‰ to -35‰). The carbon isotope composition of atmospheric CO_2 ($\delta^{13}\text{C}_{\text{atm}}$) can also be estimated using the relationship established between the $\delta^{13}\text{C}$ value of oceanic carbonates and that of atmospheric CO_2 ([Passey et al., 2002](#)):

$$\delta^{13}\text{C}_{\text{atm}} = \delta^{13}\text{C}_{\text{oceanic carbonates}} - 7.9\text{‰}$$

Because the $\delta^{13}\text{C}_{\text{oceanic carbonate}}$ value was approximately 2 ‰ during this time period ([Morettini et al., 2002](#)), the estimated $\delta^{13}\text{C}_{\text{atm}}$ value was approximately -5.9‰ during the Early Jurassic. Using equation 3, the calculated Early Jurassic MAP in Lufeng County was 965 ± 460 mm.

It is worth noting that the difference in oxygen isotopes between the apex and the cervix of the *Sinosaurus* tooth is 3.4‰ (ZGT09-1A and ZGT09-2A; Figure 6). We

1
2
3
4 332 assume that this difference may be attributed to seasonal variations in temperature or
5
6 333 precipitation. Due to the subtropical paleolatitude of the Lufeng area during the Early
7
8
9 334 Jurassic, such a change may affected by both seasonal changes in the precipitation
10
11
12 335 regime as well as by variations in temperature, as the wet season being characterized
13
14 336 by lower water $\delta^{18}\text{O}$ values as a result of the elevated amount of precipitation (the so-
15
16
17 337 called amount effect; Amiot et al., 2009; Dansgaard, 1964). However, temperature
18
19 338 may overprint this tendency by raising the $\delta^{18}\text{O}$ values of meteoric water during the
20
21
22 339 warmest months, leading to either a large seasonal amplitude in $\delta^{18}\text{O}$ values if the hot
23
24
25 340 season coincides with the dry season, or a small amplitude if the warm season
26
27 341 coincide with the rainy season.
28
29
30 342

343 5.2.2 Climatic zone characterization

344 According to the paleoclimate classification proposed by [Zhang et al. \(2016\)](#),
345 Lufeng County had a tropical savanna climate during the Early Jurassic Few
346 freshwater bivalves are found in individual areas, characterized by thick-shelled types
347 adapted to warm environments belonging to the *Eolamprotula-Cuneopsis-Psilunio*
348 faunal assemblage. In addition, pollen data *Classopllis* was observed to be of high
349 content, reflecting an arid climate ([Deng et al., 2017](#)). Today, this climate dominates
350 many low latitude regions such as parts of the African continent, the northern parts of
351 South America, Australia, and parts of Asia (e.g., India). The average annual rainfall
352 amount in this climate zone is relatively low, varying between 800 and 1,600 mm and
353 decreasing with increasing latitude ([Leong, 1995](#)). Based on modern observation, the

1
2
3
4
5
6
7
8
9
10
11
12
13
14
15
16
17
18
19
20
21
22
23
24
25
26
27
28
29
30
31
32
33
34
35
36
37
38
39
40
41
42
43
44
45
46
47
48
49
50
51
52
53
54
55
56
57
58
59
60

354 climate in tropical savannas shows alternating arid and humid seasons called wet and
355 dry climates due to the influence of trade winds. There is a huge difference in
356 precipitation between summer and winter. In summer, onshore winds bring rain, and
357 in winter, offshore winds keep the savanna arid. In the driest months of winter, the
358 precipitation amount is less than 60 mm (Leong, 1995). The average monthly
359 temperature is >18°C throughout the year, and temperatures are higher during the
360 rainy season. The temperatures are 25-30°C during the rainy season and 20-25°C
361 during the arid season (Leong, 1995).

362 Under such climate conditions, the natural vegetation in tropical savannas
363 primarily consists of tall grasses and short deciduous trees. These trees shed their
364 leaves during periods of drought to reduce the loss of water by transpiration. They
365 also tend to have wide trunks that can store additional water to help them survive
366 during prolonged drought. Local vertebrate species richness is about almost the same
367 level between tropical savannas and tropical forests (Murphy, Andersen, & Parr,
368 2016). For terrestrial animals, large size influences their movement in dense forests,
369 therefore the open environment of the savannas is more conducive to large animal
370 species. As a result, the savanna climate accommodates a wide range of animal sizes
371 and high biodiversity (Noto & Grossman, 2010). It can be inferred that the Lufeng
372 area, similarly to the current African savanna, was highly rich in biodiversity. Indeed,
373 in addition to dinosaur fossils, mammals and other vertebrates are abundant (Chow
374 and Hou, 1959; Chow, 1962; Crompton & Sun, 1985; Dong, 1990; Hopson, 1964;
375 Patterson & Olson, 1961; Rigney, 1963; Simmons, 1965; Sun & Cui, 1986; Wu 1991;

Wu & Chatterjee, 1993; Zhang & Cui, 1983). A climatic environment similar to a tropical savanna might account for the high diversity of fossil species in Lufeng. Besides, open environment like savannas are more suited for larger animals. Therefore, the Lufeng County might have a greater proportion of large-bodied taxa like basal sauropodiform and lack anything smaller than 10 kg due to its savanna-like paleoenvironment (Noto & Grossman, 2010).

5.3 Spatial relationships between dinosaur fossils and climatic regimes

Gardner et al. (2016) suggested that warm and humid conditions were beneficial to avian fossil burial after evaluating avian fossils from the Jurassic and Cretaceous. Most of the bodies suffered weathering and then underwent a long period of petrification. Warm and humid temperatures are conducive to the preservation of intact avian fossils, which contradicts the common view that drought is better for fossil preservation. Therefore, it is necessary to test the wet and dry distribution of Jurassic dinosaur fossils.

To evaluate the spatial relationship between dinosaur fossils and climatically sensitive deposits, standard deviational ellipses (SDEs) of the dinosaur fossils, arid indicators, and humid indicators are drawn for each time slice (Figure 7). An SDE is a graphical representation of the standard deviation along the X and Y axes, centred on the average geometric data for all positions. In two-dimensional space, the point distribution has two directions: (1) centralization (centralized trend) and (2) spread (dispersion). The central tendency and dispersion refer to the diffusion of the average

1
2
3
4
5
6
7
8
9
10
11
12
13
14
15
16
17
18
19
20
21
22
23
24
25
26
27
28
29
30
31
32
33
34
35
36
37
38
39
40
41
42
43
44
45
46
47
48
49
50
51
52
53
54
55
56
57
58
59
60

centre bounded by an ellipse (Rahmaniati et al., 2014). The purpose is to provide a summary of the trend and to check whether the dispersion of the data is biased against the distribution points. The rotation and intersection areas, as well as the distance of the ellipse gravity centres between the fossils and humid/arid indicators are obtained, aiming to describe the tendency of fossils distributed among different climate conditions. A smaller rotation, a larger intersection area, and a shorter distance from the centre of gravity represent a stronger correlation, and vice versa.

The following comparisons are based on arid zone vs. dinosaur occurrence and humid zone vs. dinosaur occurrence, and for ease of reading we abbreviate the former as A-D and the latter as H-D. If we represent a difference in value, we use D(A-D) for the difference value between the arid zone and dinosaur occurrence and D(H-D) for the difference value between the humid zone and dinosaur occurrence.

In Figure 8, the SDE rotation angles of D(A-D) and D(H-D) are 9.57 and 4.78 degrees during the Early-Middle Jurassic, respectively, and -8.83 and -7.93 degrees during the Late Jurassic, respectively. This suggests that the distribution of dinosaur fossils is consistent with the climate regimes and does not deviate from the general direction of the climate regimes. During the Early-Middle Jurassic, the distances between the ellipse gravity centres of D(A-D) and D(H-D) are 3.3E+6 and 5.6E+6, respectively. During the Late Jurassic, these distances are 4.5E+5 and 4.6E+6, respectively. During the Jurassic, dinosaur fossils had a closer spatial relationship to the arid regime, which suggests that an arid climate is conducive to the preservation of the dinosaur fossils. The intersection area of the SDE shows that 81% of the arid

regime and 47% of the humid regime contained dinosaur fossils from the Early-Middle Jurassic, while the shares are 85% and 38% for the Late Jurassic. This suggests that sites with arid climates would have a higher possibility of yielding dinosaur fossils.

Overall, the results of the SDEs showed that an arid climate seems to provide better conditions than does a humid climate for fossil preservation on a global scale.

426

427 **Conclusion**

The oxygen and carbon isotope compositions of dinosaur apatites recovered from Southwest China suggested that the MAT was $21 \pm 3^{\circ}\text{C}$ and the MAP was 965 ± 460 mm during the Early Jurassic. The inferred warm and dry climatic condition corroborates the tropical savannas landscape in the region as revealed by pollen and bivalves data in previous study. The tropical savannas climate indicates that the Lufeng county may develop with a distinct humid and arid season in the Early Jurassic. We also compared the spatial distribution of global dinosaur fossils with that of climatically sensitive deposits during the Jurassic. It showed that the dinosaur fossils had a strong preference for distributing over arid regions. Therefore, we suggest that relatively arid tropical savannas favoured the accommodation of a large number of dinosaurs and the preservation of such a high number of carcasses in the Lufeng area during the Early Jurassic. This study provides for the first time a quantitative climatic condition under which the dinosaurs lived in the Lufeng county.

441

Acknowledgments

We thank T. Wang from the Lufeng Dinosaurian Museum for supplying the materials. We thank Q. Wang, S. Cao, and J. Tan for their help during the fieldwork. We also want to thank L. Xing for providing helpful suggestions. This study was financially supported by the National Key R&D Plan of China (grant 2018YFE0204204), National Natural Science Foundation of China (grant 41790455), the Chinese "111" project (grant B20011), the China Geological Survey Program (grant DD20190685), and the Fundamental Research Funds for the Central Universities (grant 2652018130).

References

Amiot, R., Angst, D., Legendre, S., Buffetaut, E., Fourel, F., Adolfssen, J., ..., Lécuyer, C. (2017). Oxygen isotope fractionation between bird bone phosphate and drinking water. *The Science of Nature*, 104, 47.

Amiot, R., Kusuhashi, N., Saegusa, H., Shibata, M., Ikegami, N., Shimojima, S., ..., Lécuyer, C. (2020). Paleoclimate and ecology of Cretaceous continental ecosystems of Japan inferred from the stable oxygen and carbon isotope compositions of vertebrate bioapatite. *Journal of Asian Earth Sciences* 104602. <https://doi.org/10.1016/j.jseaes.2020.104602>

Amiot, R., Lécuyer, C., Buffetaut, E., Fluteau, F., Legendre, S., & Martineau, F. (2004). Latitudinal temperature gradient during the Cretaceous Upper Campanian-Middle Maastrichtian: $\delta^{18}\text{O}$ record of continental vertebrates. *Earth Planet. Sci. Lett.* 226, 255–272.

Amiot R, Lécuyer C, Buffetaut E, Escarguel G, Fluteau F, & Martineau F. (2006). Oxygen isotopes from biogenic apatites suggest widespread endothermy in Cretaceous dinosaurs. *Earth Planet Sci Lett.*, 246, 41–54.

- Amiot, R., Wang, X., Zhou, Z., Wang, X., Lécuyer, C., Buffetaut, E., ..., Xu, X. (2015). Environment and ecology of East Asian dinosaurs during the Early Cretaceous inferred from stable oxygen and carbon isotopes in apatite. *J. Asian Earth Sci.*, 98, 358–370.
- Amiot, R., Buffetaut, E., Le, C., Fernandez, V., Fourel, O. I. S., Cedex, V., & Cedex, P. (2009). Oxygen isotope composition of continental vertebrate apatites from Mesozoic formations of Thailand. *Geological Society, London, Special Publications*, 315(1), 271–283.
- Barrett, P.M., Upchurch, P., & Wang, X.L. (2005). Cranial osteology of *Lufengosaurus huenei* Young (Dinosauria: Prosauropoda) from the Lower Jurassic of Yunnan, People's Republic of China. *Journal of Vertebrate Paleontology*, 25, 806–822.
- Barrett, P. M., Upchurch, P., Zhou, X.D., & Wang, X.L. (2007a). The skull of *Yunnanosaurus huangi* Young, 1942 (Dinosauria: Prosauropoda) from the Lower Lufeng Formation (Lower Jurassic) of Yunnan, China. *Zoological Journal of the Linnean Society*, 150(2), 319–341.
- Barrett, P. M., & Upchurch, P. (2007b). The evolution of feeding mechanisms in early Sauropodomorph dinosaurs. *Palaeontology, Special Papers* 77, 91–112.
- Boucot, A.J., Xu, C., & Scotese, C.R. (2013). Phanerozoic paleoclimate: An atlas of lithologic indicators of climate, Phanerozoic Paleoclimate.
- Chatterjee, S., Wang, T., Pan, S.G., Dong, Z., Wu, X.C., & Upchurch, P. (2010). A complete skeleton of a basal sauropod dinosaur from the early Jurassic of China and the origin of Sauropoda. *Geological Society of America Abstracts with Programs*, 42 (5), 26.
- Chen, H., Hu, J. M., Qu, H. J., & Wu, G. L. (2011). Early Mesozoic structural deformation in the Chuandian N-S Tectonic Belt. *China. Sci. China Earth Sci.* 54, 1651–1664.
- Chow, M. (1962). A tritylodont specimen from Lufeng, Yunnan. *Vertebrata Palasiatica*, 6, 365–367.
- Chow, M., & Hou, C. C. (1959). A new tritylodont from Lufeng, Yunnan. *Vertebrata Palasiatica*, 3, 9–12.
- Craggs, H. J., Valdes, P. J. & Widdowson, M. (2012). Climate model predictions for the latest Cretaceous: An evaluation using climatically sensitive sediments as proxy indicators. *Palaeogeography, Palaeoclimatology, Palaeoecology*, 315–316(0), 12–23.
- Crompton, A. W., & Sun, A L. (1985). Cranial structure and relationships of the Liassic mammal

- 497 Sinoconodon. *Zoological Journal of the Linnean Society*, 85, 99-119.
- 498 Cullen, T. M., Longstaffe, F. J., Wortmann, U. G., Huang, L., Fanti, F., Goodwin, M. B., ...,
- 499 Evans, D. C. (2020). Large-Scale Stable Isotope Characterization of a Late Cretaceous
- 500 Dinosaur-Dominated Ecosystem. *Geology*, 48(6), 546–51.
- 501 Dansgaard, W. (1964). Stable isotopes in precipitation. *Tellus*, 16, 436–468.
- 502 Deng, S. H., Lu, Y. Z., Zhao, Y., Fan, R., Wang, Y. D., Yang, X. J., ..., Sun, B. N. (2017). The
- 503 Jurassic paleoclimate regionalization and evolution of China. *Earth Science Frontiers*,
- 504 24(1), 106–142.
- 505 Diefendorf, A. F., Mueller, K. E., Wing, S. L., Koch, P. L., & Freeman, K. H. (2010). Global
- 506 patterns in leaf ^{13}C discrimination and implications for studies of past and future climate.
- 507 *Proc. Natl. Acad. Sci.*, 107, 5738–5743.
- 508 Dong, Z. M. (1990). Stegosaur of Asia. In: Carpenter K and Currie P J, eds. *Dinosaur*
- 509 *Systematics*. Cambridge University Press, Cambridge. 255-268.
- 510 Fang, X., Long, Q., Lu, L., Zhang, Z., Pan, S., Wang, Y., ..., Cheng, Z. (2000). Lower, Middle,
- 511 and Upper Jurassic subdivision in the Lufeng region, Yunnan Province. In *Third National*
- 512 *Stratigraphical Congress of China*, 208–214. Geological Publishing House Beijing.
- 513 Fricke, H.C., & O'Neil, J.R. (1999). The correlation between $^{18}\text{O}/^{16}\text{O}$ ratios of meteoric water and
- 514 surface temperature: its use in investigating terrestrial climate change. *Earth Planet. Sci.*
- 515 *Lett.*, 170, 181–196.
- 516 Fricke, H.C., & Rogers, R. R. (2000). Multiple taxon-multiple locality approach to providing
- 517 oxygen isotope evidence for warm-blooded theropod dinosaurs. *Geology*, 28, 799–802.
- 518 Fricke, H.C., & Pearson, D. A. (2008). Stable isotope evidence for changes in dietary niche
- 519 partitioning among hadrosaurian and ceratopsian dinosaurs of the Hell Creek Formation,
- 520 North Dakota. *Paleobiology*, 34, 534–552.
- 521 Galton, P. M. (1985). Diet of prosauropod dinosaurs from the late Triassic and early Jurassic.
- 522 *Lethaia*, 18, 105-123.
- 523 Galton, P. M., & Upchurch, P. (2004). In *The Dinosauria*, Second Edition (eds Weishampel, D. B.,
- 524 Dodson, P. & Osmólska, H.). CA: University of California Press, 232–258.
- 525 Hopson, J. A. (1964). The braincase of the advanced mammal- like reptile Bienotherium. *Postilla*,
- 526 87,1-30.

- 527 Hu, S. J. (1993). A short report on the occurrence of Dilophosaurus from Jinning County, Yunnan
528 Province. *Vertebrata Palasiatica*, 31: 65–69.
- 529 Huang, B. C. (2005). Jurassic magnetic stratigraphy in Lufeng area, central Yunnan. *Chinese
530 geological bulletin*, 24, 322–328. (In Chinese)
- 531 Hut, G. (1987). Consultants' group meeting on stable isotope reference samples for geochemical
532 and hydrological investigations. *Journal of Geophysical Research*, 42.
- 533 Irmis, R.B. & Knoll, F. (2008). New ornithischian dinosaur material from the Lower Jurassic
534 Lufeng Formation of China. *Neues Jahrbuch für Geologie und Paläontologie,
535 Abhandlungen*, 247, 117–128.
- 536 Izart, A., Palhol, F., Gleixner, G., Elie, M., Blaise, T., Suarez-Ruiz, I., ..., Panova, E. A. (2012).
537 Palaeoclimate reconstruction from biomarker geochemistry and stable isotopes of n-
538 alkanes from Carboniferous and Early Permian humic coals and limnic sediments in
539 western and eastern Europe. *Organic geochemistry*, 43, 125–149.
- 540 Koch, P. L., Tuross, N., & Fogel, M. L. (1997). The effects of sample treatment and diagenesis on
541 the isotopic integrity of carbonate in biogenic hydroxylapatite. *Journal of Archaeological
542 Science*, 24, 417–429.
- 543 Kohn, M. J., & Cerling, T.E. (2002). Stable Isotope Compositions of Biological Apatite. *Mineral.
544 Geochemistry*, 48, 455–488.
- 545 Kohn, M. J., Schoeninger, M. J., & Valley, J. W. (1996). Herbivore tooth oxygen isotope
546 compositions: effects of diet and physiology. *Geochimica et Cosmochimica Acta*, 60 (20),
547 3889–3896.
- 548 Kolodny, Y., Luz, B., & Navon, O. (1983). Oxygen isotope variations in phos- phate of biogenic
549 apatites, I. Fish bone apatite—rechecking the rules of the game. *Earth Planet Sci Lett.*, 64,
550 398–404.
- 551 Langer, M. C., Bittencourt, J. S., & Schultz, C. L. (2010). A reassessment of the basal dinosaur
552 Guaibasaurus candelariensis, from the Late Triassic Caturrita Formation of south Brazil.
553 *Earth and Environmental Science Transactions of the Royal Society of Edinburgh*, 101,
554 301–332.
- 555 Lécuyer, C. (2004). Oxygen Isotope Analysis of Phosphate, in: Handbook of Stable Isotope
556 Analytical Techniques. Elsevier, Amsterdam, 482–496.

- 557 Lécuyer, C., Grandjean, P., & Sheppard, S. M. F. (1999). Oxygen isotope exchange between
 558 dissolved phosphate and water at temperatures $\leq 135^{\circ}\text{C}$: inorganic versus biological
 559 fractionations. *Geochim Cosmochim Acta*, 63, 855-862.
- 560 Lécuyer, C., Bogey, C., Garcia, J.P., Grandjean, P., Barrat, J.A., Floquet, M., ..., Pereda-
 561 Superbiola, X. (2003). Stable isotope composition and rare earth element con- tent
 562 of vertebrate remains from the Late Cretaceous of northern Spain (Laño): did the
 563 environmental record survive? *Palaeogeography, Palaeoclimatology, Palaeoecology*, 193,
 564 457–471.
- 565 Lécuyer, C., Grandjean, P., O'Neil, J.R., Capetta, H., & Martineau, F. (1993). Thermal excursions
 566 in the ocean at the Cretaceous–Tertiary boundary (northern Morocco): the $\delta^{18}\text{O}$ record of
 567 phosphatic fish debris. *Palaeogeogr. Palaeoclimatol. Palaeoecol*, 105, 235-243.
- 568 Leong G. C. (1995). Certificate Physical and Human Geography. *Oxford; 1st edition (October 1,*
 569 *1995).*
- 570 Longinelli, A. (1984). Oxygen isotopes in mammal bone phosphate: a new tool for
 571 paleohydrological and paleoclimatological research? *Geochim Cosmochim Acta*, 48, 385–
 572 390.
- 573 Luo, Z. X., & Wu, X. C. (1994). The small tetrapods of the Lower Lufeng Formation, Yunnan,
 574 China; pp. 251-270 in N. C. Fraser and H-D. Sues (eds.), *In the Shadow of the Dinosaurs:*
 575 *Early Mesozoic Tetrapods.* Cambridge University Press, Cambridge.
- 576 Luz, B., Kolodny, Y., & Horowitz, M. (1984) Fractionation of oxygen isotopes between
 577 mammalian bone-phosphate and environmental drinking water. *Geochim Cosmochim*
 578 *Acta*, 48, 1689–1693.
- 579 Morettini, E., Santantonio, M., Bartolini, A., Cecca, F., Baumgartner, P.O., & Hunziger, J.C.
 580 (2002). Carbon isotope stratigraphy and carbonate production during the Early Jurassic:
 581 examples from the Umbria-Marche-Sabina Appenines (central Italy). *Palaeogeogr.*
 582 *Palaeoclimatol. Palaeoecol.*, 184, 251–273.
- 583 Murphy, B. P., Andersen, A. N., & Parr, C. L. (2016). The underestimated biodiversity of tropical
 584 grassy biomes. *Philosophical Transactions of the Royal Society B: Biological Sciences*,
 585 371(1703).
- 586 Passey, B. H., Robinson, T.F., Ayliffe, L. K., Cerling, T. E., Sponheimer, M., Dearing, M. D., ...,

- 587 Ehleringer, J.R. (2005). Carbon isotope fractionation between diet, breath CO₂, and
588 bioapatite in different mammals. *Journal of Archaeological Science*, 32(10): 1459–1470.
- 589 Passey, B. H., Cerling, T. E., Perkins, M. E., Voorhies, M. R., Harris, J. M., & Tucker, S. T.
590 (2002). Environmental Change in the Great Plains: An Isotopic Record from Fossil
591 Horses. *The Journal of Geology*, 110(4), 123–140.
- 592 Patterson, B., & Olson, E. C. (1961). A triconodont mammal from the Triassic of Yunnan. In
593 Vandebroek G, ed. International Colloquium on the Evolution of Lower and Non-
594 specialized Mammals.
- 595 Porada, P., Lenton, T. M., Pohl, A., Weber, B., Mander, L., Donnadieu, Y., ... & Kleidon, A.
596 (2016). High potential for weathering and climate effects of non-vascular vegetation in the
597 Late Ordovician. *Nature Communications*, 7(1), 1-13.
- 598 Rahmaniati, M., Eryando, T., Susanna, D., Pratiwi, D., Nugraha, F., & Riandi, U. (2014). The
599 utilization of Standard Deviation Ellipse (SDE) model for the analysis of dengue fever
600 cases in Banjar city 2013. *Aspirator*, 6, 21–28.
- 601 Rey, K. vin, Amiot, R., & Fourel, F. (2017). Oxygen isotopes suggest elevated thermometabolism
602 within multiple Permo-Triassic therapsid clades Oxygen isotopes suggest elevated
603 thermometabolism within multiple Permo- Triassic therapsid clades. *eLife Sci*.
- 604 Rigney, H. W. (1963). A specimen of Morganucodon from Yunnan. *Nature*, 197, 1122-1123.
- 605 Sekiya, T. (2010). A new prosauropod dinosaur from Lower Jurassic in Lufeng of Yunnan. *Global*
606 *Geology*, 29, 6–15.
- 607 Simmons, D. J. (1965). The non-therapsid reptiles of the Lufeng Basin, Yunnan, China. *Fieldiana:*
608 *Geology*, 15, 1-93.
- 609 Spoetl, C., & Vennemann, T.W. (2003). Continuous-flow isotope ratio mass spectrometric
610 analysis of carbonate minerals. *Rapid Commun. Mass Spectrom.*, 17, 1004–1006.
- 611 Stanton-Thomas, K.J., & Carlson, S.J. (2004). Microscale $\delta^{18}\text{O}$ and $\delta^{13}\text{C}$ isotopic analysis of an
612 ontogenetic series of the hadrosaurid dinosaur Edmontosaurus: Implications for
613 physiology and ecology. *Palaeogeogr Palaeoclimatol Palaeoecol.*, 206, 257–287.
- 614 Straight, W. H., Barrick, R. E., & Eberth, D. A. (2004). Reflections of surface water, seasonality
615 and climate in stable oxygen isotopes from tyrannosaurid tooth enamel. *Palaeogeography,*
616 *Palaeoclimatology, Palaeoecology.*, 206(3-4), 239-256.

- 617
- 618 Sun, A. L., & K. H. Cui. (1986). A brief introduction to the Lower Lufeng saurischian fauna
619 (Lower Jurassic: Lufeng, Yunnan. People's Republic of China), 275-278 in K. Padian
620 (ed.), *The Beginning of the Age of Dinosaurs: Faunal Change Across the Triassic-Jurassic*
621 *Boundary*. Cambridge University Press, Cambridge.
- 622 Torsvik, T. H. & Cocks, L. R. M. (2016). *Earth history and palaeogeography*. Cambridge
623 University Press.
- 624 Tütken, T., Pfretzschner, H. U., Vennemann, T. W., Sun, G., & Wang, Y. D. (2004). Paleobiology
625 and skeletochronology of Jurassic dinosaurs: Implications from the histology and oxygen
626 isotope compositions of bones. *Palaeogeogr. Palaeoclimatol. Palaeoecol.*, 206, 217–238.
- 627 Tütken, T. (2011). The diet of sauropod dinosaurs: implications from carbon isotope analysis of
628 teeth, bones, and plants, in: Klein, N., Remes, K., Sander, M. (Eds.), *Biology of the*
629 *Sauropod Dinosaurs: Understanding the Life of Giants*. Indiana University Press,
630 Bloomington, 57–79.
- 631 Utescher, T., Ashraf, A. R., Kern, A. K., & Mosbrugger, V. (2020). Diversity patterns in
632 microfloras recovered from Miocene brown coals of the lower Rhine Basin reveal distinct
633 coupling of the structure of the peat - forming vegetation and continental climate
634 variability. *Geological Journal*.
- 635 Vennemann, T. W., Hegner, E., Cliff, G., & Benz, G. W. (2001). Isotopic composition of recent
636 shark teeth as a proxy for environmental conditions. *Geochimica Et Cosmochimica Acta*,
637 65, 1583–1599.
- 638 Grafenstein, U. V., Erlenkeuser, H., Mueller, J., Trimborn, P., & Alefs, J. (1996). A 200 year mid-
639 European air temperature record preserved in lake sediments; an extension of the $\delta^{18}\text{O}_{\text{P}}$ -
640 air temperature relation into the past. *Geochim. Cosmochim. Acta*, 60, 4025–4036.
- 641 Wang, Y. M., You, H. L., & Wang, T. (2017). A new basal sauropodiform dinosaur from the
642 Lower Jurassic of Yunnan Province, China. *Sci. Rep.*, 7, 41881.
- 643 William, W. H., & Sascha, F. (2012). New thoughts about the Cretaceous climate and oceans.
644 *Earth-Science Reviews*, 115, 262-272.
- 645 Wu, X., Currie, P.J., Dong, Z., Pan, S., & Wang, T. (2009). A new theropod dinosaur from the
646 Middle Jurassic of Lufeng, Yunnan, China. *Acta Geologica Sinica*, 83, 9–24 (In Chinese).

- 647 Wu, X. C. (1991). The comparative anatomy and systematics of Mesozoic sphenodontidans. Ph.D.
648 dissertation, McGill University, Montreal, 229.
- 649 Wu, X. C., & Chatterjee, S. (1993). *Dibothrosuchus elaphros*, a crocodylomorph from the Lower
650 Jurassic of China and the phylogeny of the Sphenosuchia. *Journal of Vertebrate*
651 *Paleontology*, 13 (1), 58-89.
- 652 Noto, C. R., & Grossman, A. (2010). Broad scale patterns of Late Jurassic dinosaur paleoecology.
653 PLoSONE5: e12553.
- 654 Xing, L.D., Bell, P.R., Rothschild, B.M., Ran, H., Zhang, J.P., Dong, Z.M., ..., Currie, P.J. (2013).
655 Tooth loss and alveolar remodeling in *Sinosaurus triassicus* (Dinosauria: Theropoda) from
656 the lower jurassic strata of the Lufeng Basin, China. *Chinese Sci. Bull.*, 58, 1931–1935.
- 657 Young, C. C. (1941a). A complete osteology of *Lufengosaurus huenei* Young (gen. et sp. nov.)
658 from Lufeng, Yunnan, China. *Palaeontologica Sinica (Series C)*, 7, 1–53.
- 659 Young, C. C. (1941b). *Gyposaurus sinensis* (sp. nov.), a new Prosauropoda from the Upper
660 Triassic beds at Lufeng, Yunnan. *Bulletin of Geology Society of China*, 21, 205-253.
- 661 Young, C. C. (1942). *Yunnanosaurus huangi* (gen. et sp. nov.), a new Prosauropoda from the Red
662 Beds at Lufeng, Yunnan. *Bulletin of the Geological Society of China*, 22, 63-104.
- 663 Young, C. C. (1947). On *Lufengosaurus magnus* Young (sp. nov.) and additional finds of
664 *Lufengosaurus huenei* Young. *Palaeontologica Sinica (Series C)*, 12, 1-53.
- 665 Young, C.C. (1951). The Lufeng saurischian fauna. *Palaeontologica Sinica (Series C)*, 13, 1–96.
- 666 Zazzo, A., Lécuyer, C., & Mariotti, A. (2004a). Experimentally-controlled carbon and oxygen
667 isotope exchange between bioapatites and water under inorganic and microbially-mediated
668 conditions. *Geochim Cosmochim Acta*, 68, 1–12.
- 669 Zazzo, A., Lécuyer, C., Sheppard, S. M. F., Grandjean, P., & Mariotti, A. (2004b). Diagenesis and
670 the reconstruction of paleoenvironments: a method to restore original d¹⁸O values of
671 carbonate and phosphate from fossil tooth enamel. *Geochimica Et Cosmochimica Acta.*,
672 68, 2245–2258.
- 673 Zhang, F., & Cui, G. (1983). New material and new understanding of *Sinoconodon*. *Vertebrata*
674 *Palasiatica*, 21, 32-41.
- 675 Zhang, L., Wang, C., Li, X., Cao, K., Song, Y., Hu, B., ..., Cao, S. (2016). A new paleoclimate
676 classification for deep time. *Palaeogeogr. Palaeoclimatol. Palaeoecol.*, 443, 98–106.

1
2
3
4
5
6
7
8
9
10
11
12
13
14
15
16
17
18
19
20
21
22
23
24
25
26
27
28
29
30
31
32
33
34
35
36
37
38
39
40
41
42
43
44
45
46
47
48
49
50
51
52
53
54
55
56
57
58
59
60

677 Zhang, Y. H., & Yang, Z. L. (1995). A new complete osteology of Prosauropoda in Lufeng Basin,
678 Yunnan, China: Jingshanosaurus. (Yunnan Publishing House of Science and Technology).

For Peer Review

Figure Captions

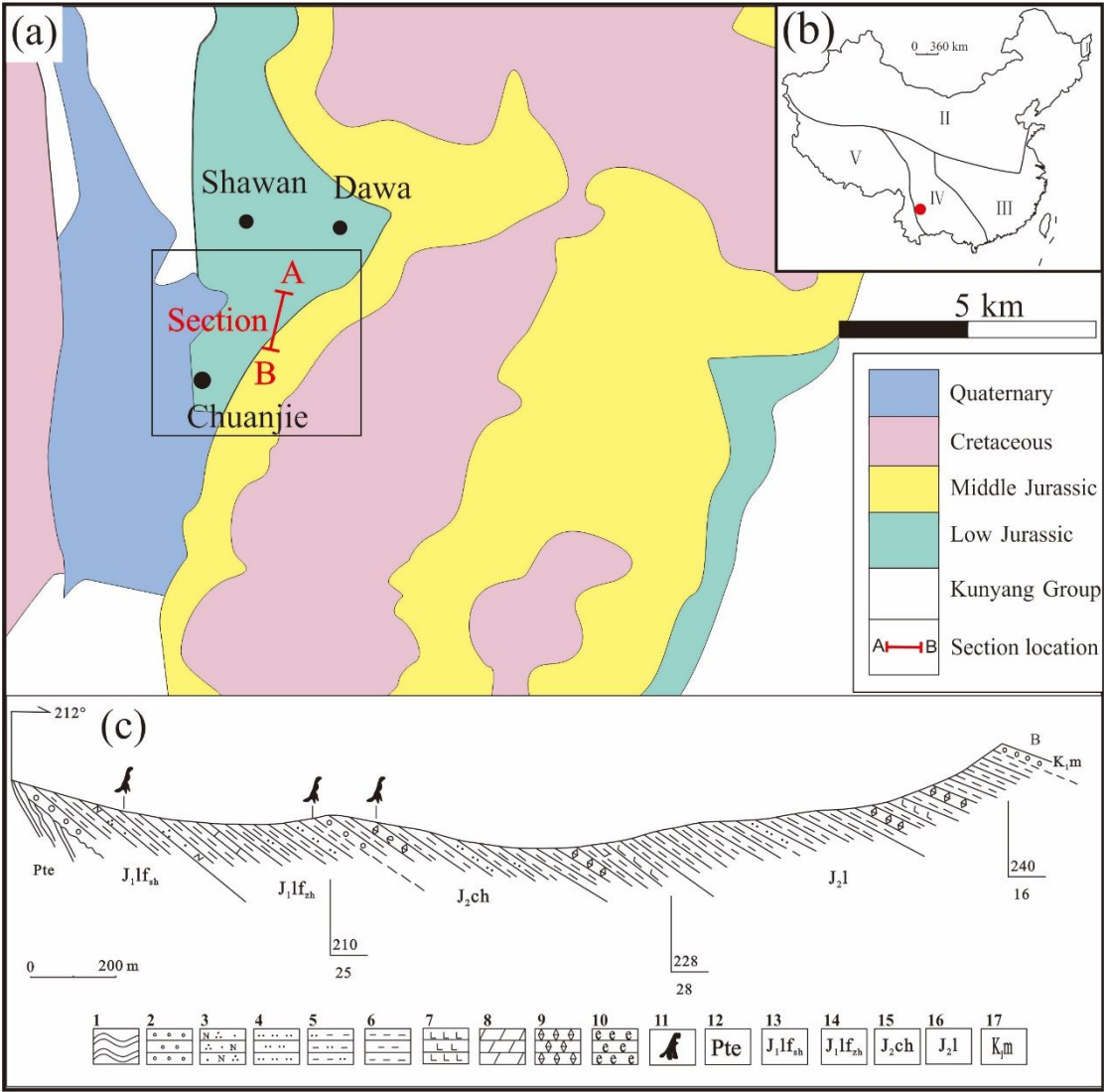


Figure 1 Schematic geological map of the Lufeng Basin. (a) The geological setting of the Lufeng Basin. (c) The study section from A to B. 1 Killas; 2 Basal conglomerates; 3 Arkosic sandstone; 4 Siltstone; 5 Argillaceous siltstones; 6 Mudstone; 7 Calcareous mudstones; 8 Marlstone; 9 Micritic limestones; 10 Bioclastic limestone; 11 Dinosaur fossils; 12 Kunyang group; 13 Shawan member in Low Jurassic; 14 Zhangjiaao member in Low Jurassic; 15 Chuanjie member in Middle Jurassic; 16 Laoluocun member in Middle Jurassic; 17 Matoushan Formation in Cretaceous. Modified after Wang et al. (2017) and Fang et al. (2000). (b) The Jurassic climatic zones in China, modified after Deng et al. (2007). (I) Wushuli warm-cool climatic region in Eastern Heilongjiang, (II) North China warm-temperate humid climatic region, (III) Southeast China tropic-subtropical humid climatic region, (IV)

1
2
3
4
5
6
7
8
9
10
11
12
13
14
15
16
17
18
19
20
21
22
23
24
25
26
27
28
29
30
31
32
33
34
35
36
37
38
39
40
41
42
43
44
45
46
47
48
49
50
51
52
53
54
55
56
57
58
59
60

689 Southwest China tropic-subtropical semi-arid and semi-humid climatic region, (V) Tibetwestern Yunnan tropical
690 oceanic arid climatic region.

For Peer Review

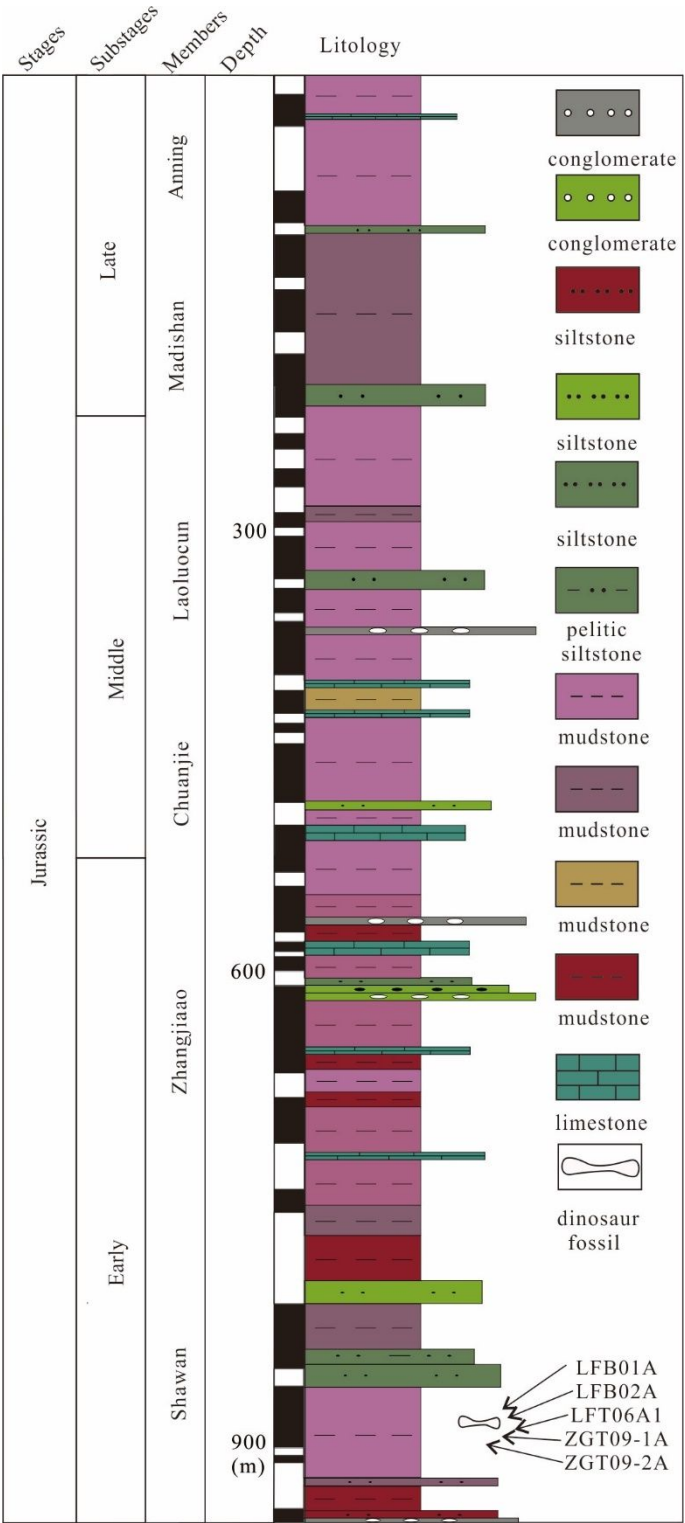


Figure 2 Lithological column of the Lufeng Basin. The samples were recovered from the lower part of the Shawan Member.

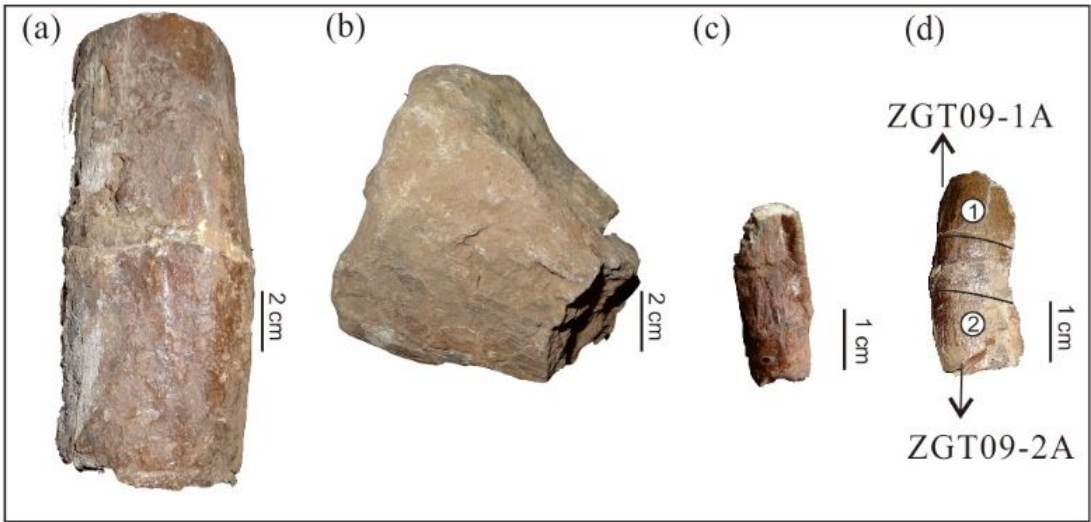


Figure 3 Teeth and bones analysed in this study. (a-b) The basal sauropodiform dinosaur bones; (c) The basal sauropodiform dinosaur tooth; (d) The *S. triassicus* tooth.

Table 1 The oxygen isotope compositions of dinosaurs' phosphate and carbonate.

Sample ID	Material	Taxa	Ecology ^a	$\delta^{18}\text{O}_p$ (‰, VSMOW)		$\delta^{13}\text{C}_{\text{CO}_3}$ (‰, VPDB)		$\delta^{18}\text{O}_{\text{CO}_3}$ (‰, VSMOW)		CaCO_3 (Wt%)
				$\delta^{18}\text{O}_{\text{cor}}$	SD	$\delta^{13}\text{C}_{\text{CO}_3}$	SD	$\delta^{18}\text{O}_{\text{CO}_3}$	SD	
LFB01A	bone	basal sauropodiform	herb.	15.9	0.1	-10.6	0.1	19.9	0.1	3.1
LFB02A	bone	basal sauropodiform	herb.	16.4	0.1	-9.2	0.1	21.5	0.1	2.1
LFT06A1	teeth crown	basal sauropodiform	herb.	20.5	0.2	-8.7	0.1	23.7	0.1	2.6
ZGT09-1A	teeth apex	Sinosaurus	carn.	20.4	0.2	-7.8	0.1	27.2	0.1	12.1
ZGT09-2A	teeth cervix	Sinosaurus	carn.	17.0	0.1	-7.1	0.1	21.0	0.1	2.6

^a *herb.* Herbivorous, *carn.* Carnivorous.

1
2
3
4
5
6
7
8
9
10
11
12
13
14
15
16
17
18
19
20
21
22
23
24
25
26
27
28
29
30
31
32
33
34
35
36
37
38
39
40
41
42
43
44
45
46
47
48
49
50
51
52
53
54
55
56
57
58
59
60

700

Table 2 The mean values of $\delta^{18}\text{O}_w$ and MAT in Lufeng Locality

Taxa	$\delta^{18}\text{O}_{\text{PO}_4}$ (‰, VSMOW)		$\delta^{18}\text{O}_{\text{PO}_4}$ (‰, VSMOW)		Estimated $\delta^{18}\text{O}_w$ (‰, VSMOW)		MAT (°C)	
	Mean	SD	Mean	SD	Mean	SD	Mean	SD
basal sauropodiform dinosaur	17.6	0.2	18.2	0.3	-3.9	±0.7	21	±0.8
S.triassicus	18.7	0.2						

For Peer Review

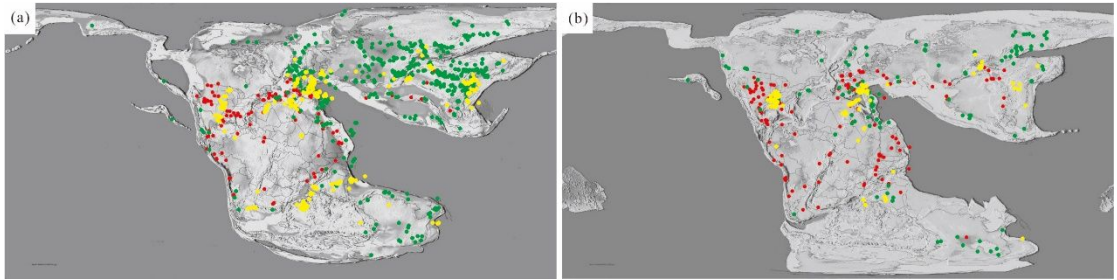


Figure 4. The distributions of dinosaur fossils and climatically sensitive sediments during the (a) Early - middle Jurassic and (b) Late Jurassic. The yellow dots represent the dinosaur fossil sites. The red and green dots represent the arid and humid climatically sensitive deposits, respectively.

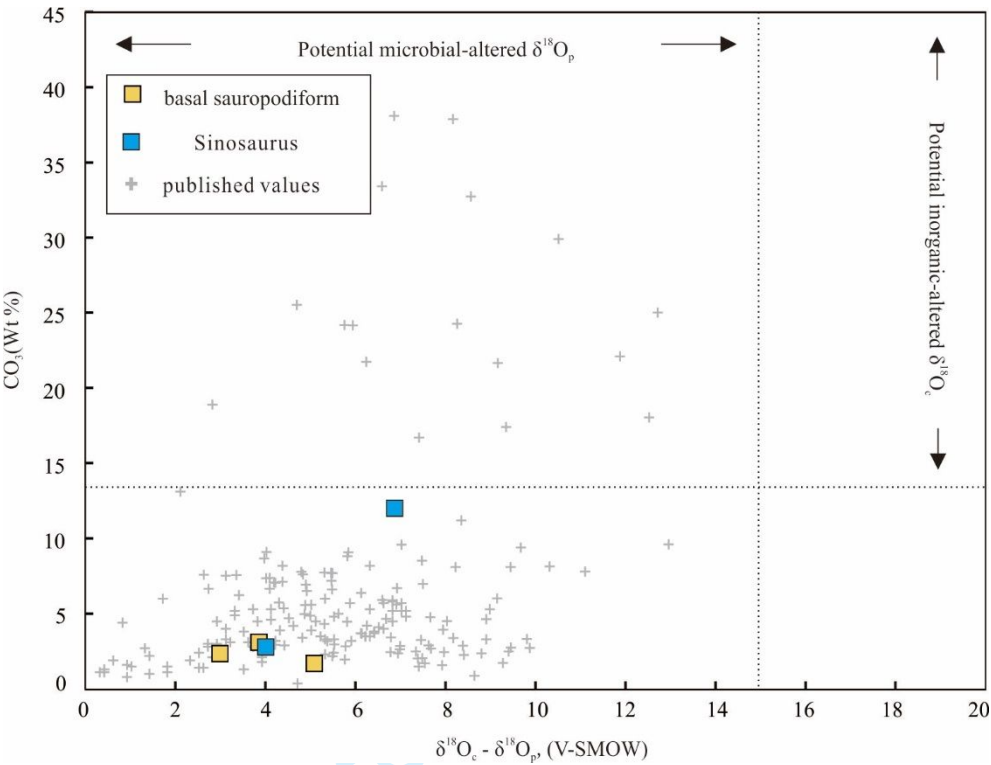


Figure 5 The assessment of the preservation condition. The $\delta^{18}\text{O}_c - \delta^{18}\text{O}_p$ differences between teeth and bones plotted against the structural carbonate content (wt %) of apatite. Modified after Amiot et al. (2015) and Rey et al. (2017).

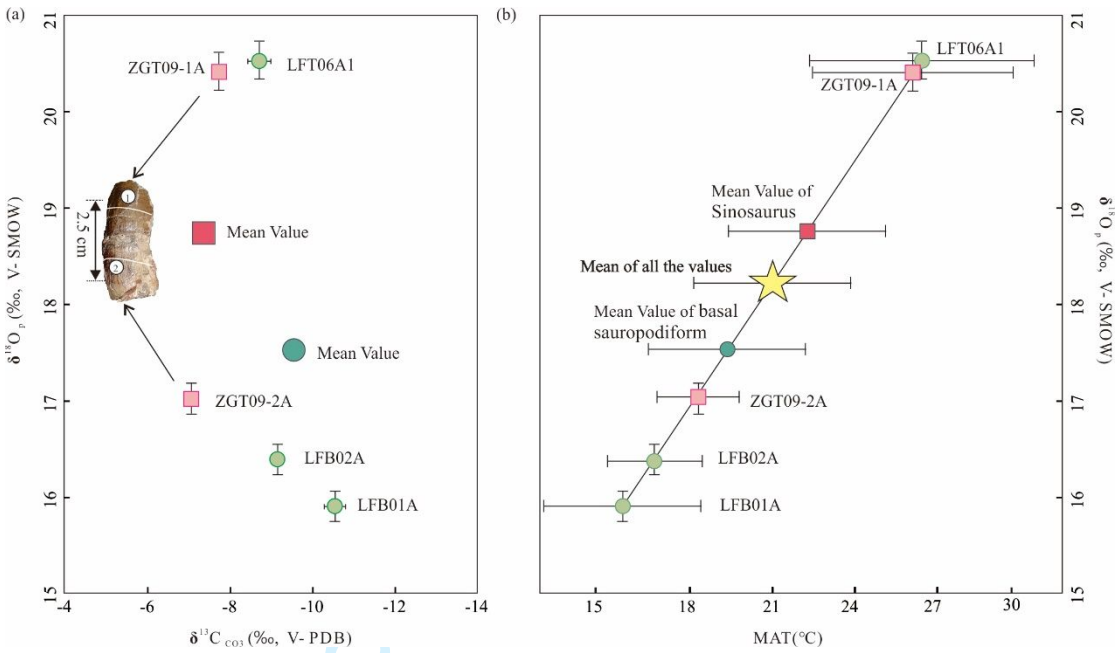


Figure 6 The stable isotope compositions of the dinosaur fossils. (a) The mean $\delta^{18}O_p$ (‰, VSMOW) vs $\delta^{13}C_{CO_3}$ (‰, VPDB) values. (b) The temperature vs $\delta^{18}O_p$ (‰, VSMOW). The red squares represent Sinosaurus tooth, the green circles represent the basal sauropodomorphs, and the yellow star represents the mean MAT.

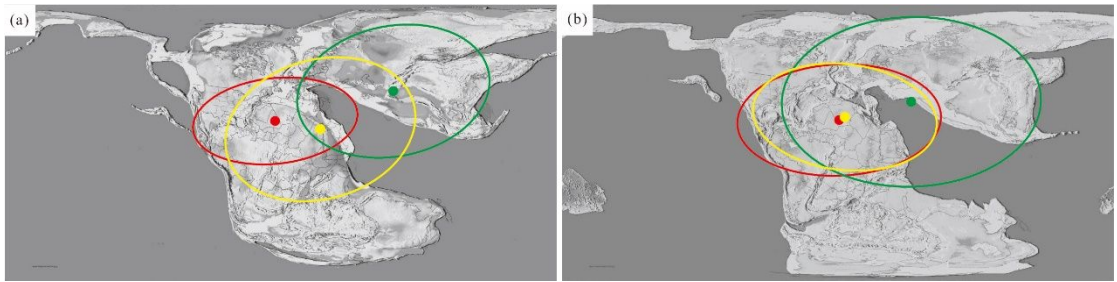


Figure 7 The standard elliptic and center of gravity of dinosaur and climatic proxies. (a) Early-middle Jurassic and (b) Late Jurassic. The yellow elliptic represents dinosaur data. The red elliptic represents the arid climatic data and the green represents humid climatic data. The corresponding colored circles represent the position of the center of elliptic gravity.

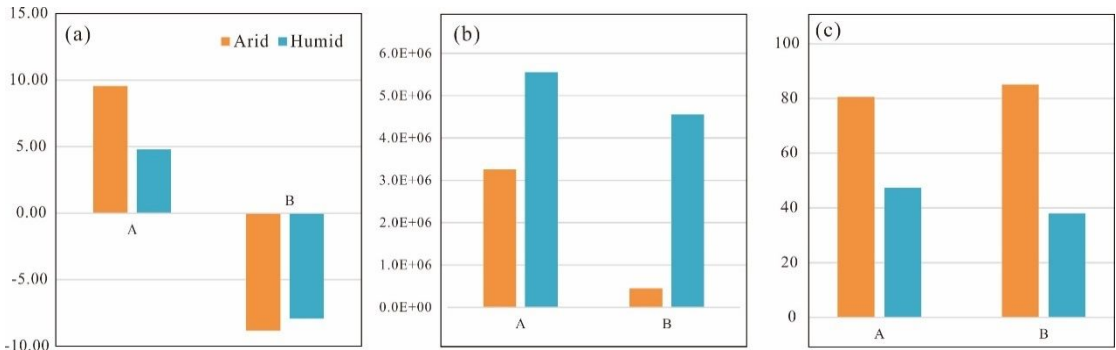


Figure 8 Summarizes the bar chart of SDE spatial analysis in Jurassic. (a) Bar chart of SDE rotation of D(A-D) and D(H-D). (b) Bar chart of the distance between the SDE gravity of A-D and H-D. (c) Bar chart of percentage between the intersection area of A-D and H-D.